Earth and Planetary Science Letters xxx (2011) xxx–xxx

Contents lists available at ScienceDirect

Earth and Planetary Science Letters

journal homepage: www.elsevier.com/locate/epsl

Sea-level and salinity fluctuations during the Paleocene–Eocene thermal maximum in Arctic Spitsbergen

Ian C. Harding [a,*], Adam J. Charles [a], John E.A. Marshall [a], Heiko Pälike [a], Andrew P. Roberts [b], Paul A. Wilson [a], Edward Jarvis [a,c], Robert Thorne [a], Emily Morris [a], Rebecca Moremon [a], Richard B. Pearce [a], Shir Akbari [a]

[a] School of Ocean and Earth Science, National Oceanography Centre Southampton, University of Southampton, European Way, Southampton, SO14 3ZH, UK
[b] Research School of Earth Sciences, The Australian National University Canberra, ACT 0200, Australia
[c] Fugro-Robertson, Pen-y-coed, Llanrhos, Llandudno, North Wales, UK

ARTICLE INFO

Article history:
Received 4 July 2010
Received in revised form 15 December 2010
Accepted 20 December 2010
Available online xxxx

Editor: P. DeMenocal

Keywords:
abrupt/rapid climate change
PETM
paleoecology
sedimentology
Spitsbergen
Arctic

ABSTRACT

Palaeoenvironmental manifestations of the Paleocene–Eocene thermal maximum (PETM; ~56 Ma) are relatively well documented in low- to mid-latitude settings and at high southern latitudes, but no documented high northern latitude sites record the entire hyperthermal event. We present high-resolution multi-proxy records from a PETM succession on Spitsbergen in the high Arctic (palaeolatitude ~75 °N). By comparing our results with those from Integrated Ocean Drilling Program Site 302-4A, we document regional palaeoenvironmental variations in the expression of the PETM, with evidence for major differences in basin-margin vegetation and water column oxygen depletion. Sedimentological, palynological and geochemical data demonstrate a pre-PETM sea level rise in Spitsbergen before the −4‰ $\delta^{13}C_{TOC}$ excursion, which culminated in maximum flooding during the peak of the event. The appearance of the dinoflagellate cyst *Apectodinium* before the onset of the carbon isotope excursion (CIE) corroborates that environmental change in the Arctic had begun prior to the CIE. Sedimentological and palynological evidence indicate that elevated terrestrial runoff resulted in water column stratification, providing further evidence for an intensification of the hydrological cycle during the PETM.

1. Introduction

The Paleocene–Eocene Thermal Maximum (PETM: Kennett and Stott, 1991; Sluijs et al., 2007a; Zachos et al., 2001, 2003, 2005) was an abrupt but transient episode of global warming which occurred at about 56 Ma (Westerhold et al., 2009) and lasted for ~170 kyr (Abdul Aziz et al., 2008; Röhl et al., 2007). The temperature rise is recorded by oxygen isotope excursions in both foraminiferal calcite (Kennett and Stott, 1991; Thomas and Shackleton, 1996; Thomas et al., 2002) and palaeosol carbonates (Koch et al., 1995; Magioncalda et al., 2004) by an increase in Mg/Ca in foraminiferal calcite (Tripati and Elderfield, 2005; Zachos et al., 2003), and by organic geochemical temperature proxies in both marine and terrestrial settings (Sluijs et al., 2006; Weijers et al., 2007; Zachos et al., 2006). Evidence for elevated temperatures is associated with a pronounced negative carbon isotope ($\delta^{13}C$) excursion (CIE) of 2.5 to 6‰ (e.g. Kennett and Stott, 1991; Koch et al., 1992; Pagani et al., 2006; Thomas et al., 2002), which marks the start of the Eocene Epoch. The CIE is recorded in both marine and terrestrial carbonates (Bowen et al., 2001, 2004; Koch et al., 1992) and in marine- and terrestrially derived organic carbon (John et al., 2008; Magioncalda et al., 2004), including higher plant alkanes (Handley et al., 2008; Pagani et al., 2006), and is widely accepted as having resulted from the rapid injection of ^{13}C-depleted carbon (as CO_2 and/or CH_4), into the global exogenic carbon pool (Dickens et al., 1995).

Perturbation of the global climate system during the PETM resulted in major biotic turnovers and migrations, including the most severe marine benthic foraminiferal extinction of the Cenozoic (Thomas, 1998; Thomas and Shackleton, 1996), and a poleward migration of (sub-) tropical plankton (Crouch et al., 2001; Kelly et al., 1996), such as the dinoflagellate cyst genus *Apectodinium* (Bujak and Brinkhuis, 1998; Sluijs et al., 2008a). A similar response is recorded in terrestrial environments, with the migration of plants (Wing et al., 2005) and mammals (Bowen et al., 2002; Smith et al., 2006) to higher latitudes. Surface and deep ocean water temperatures were both subject to increases of ~5 °C during the PETM (Tripati and Elderfield, 2005; Zachos et al., 2003), with eustatic sea level calculated to have risen by 3–5 m, as a result of thermal expansion of seawater (Sluijs et al., 2008b). Biotic, grain size and organic geochemical data from four continents provide evidence for a third-order sea level transgression during the lower part of Chron C24r, coincident with the PETM (Sluijs et al., 2008b). Such a rise in sea level may have been amplified by the melting of small-scale late Paleocene icesheets that have been invoked in various studies (e.g. DeConto and Pollard, 2003; Miller et al., 2005).

* Corresponding author.
E-mail address: ich@noc.soton.ac.uk (I.C. Harding).

0012-821X/$ – see front matter © 2010 Elsevier B.V. All rights reserved.
doi:10.1016/j.epsl.2010.12.043

Although multiple PETM sites have been documented from low- to mid-latitude and high southern latitude sites, there are still few PETM records from high northern latitudes (Sluijs et al., 2006, 2008a; Weijers et al., 2007). The lack of data from such locations has partly been due to a paucity of available sections, and partly due to imprecise temporal constraints for studied continental successions (Bice et al., 1996; Greenwood and Wing, 1995; Markwick, 1998; Tripati et al., 2001). The one high northern latitude PETM succession documented in detail is IODP Site 302-4A (Moran et al., 2006) that was drilled at ~88°N beneath Arctic pack ice on the Lomonosov Ridge. Site 302-4A has provided a wealth of information on the nature of the PETM in the Arctic Basin (Knies et al., 2008; Pagani et al., 2006; Schouten et al., 2007; Sluijs et al., 2006, 2008a; Waddell and Moore, 2008; Weijers et al., 2007; Weller and Stein, 2008), and in the absence of other records it has become the standard reference point for Arctic palaeoenvironmental conditions during the PETM. However, the Site 302-4A record is incomplete with no core recovery from the onset and peak of the hyperthermal (Sluijs et al., 2006). These phases therefore remain undocumented in the Arctic.

Thus, in order to provide a better understanding of Arctic PETM environmental conditions, and to constrain global circulation models (GCMs), additional data from other high northern latitude sites are essential. Here we report a high latitude (78 °N) expanded and continuous nearshore shelf Palaeogene succession from Spitsbergen, the largest island in the Svalbard archipelago (Fig. 1a). The Spitsbergen Central Basin (Fig. 1c) is an ideal location to document temporal environmental changes associated with the PETM, because high sedimentation rates created a Palaeogene succession approaching 2.5 km in thickness.

2. Materials and methods

2.1. Geological succession

The Spitsbergen Central Basin developed as a syn-orogenic foreland basin east of the West Spitsbergen Orogen, the major Palaeogene fold-thrust belt that resulted from dextral strike-slip movements between Greenland and Svalbard during opening of the northernmost Atlantic Ocean (Fig. 1b; Bruhn and Steel, 2003; Harland, 1997). This led to oblique Palaeogene collision and a transpressive tectonic regime (Harland, 1997), with sediment provenance from an eastern flexural bulge (Bruhn and Steel, 2003). Subsequent uplift of the West Spitsbergen Fold-Thrust Belt shifted the source of clastic supply to a western source in the latest Paleocene, with eastward migration of deposition (Bruhn and Steel, 2003; Dallmann et al., 1999; Harland, 1997). Throughout this time, Svalbard remained at polar palaeolatitudes (~75 °N; Harland, 1997).

Although local Spitsbergen lithostratigraphic terminology has varied, we follow that of Dallmann et al. (1999). The Palaeogene Van Mijenfjorden Group consists of clastic sediments, dominantly sandstones and shales with coal-bearing units at its base and top, that represent delta-influenced shelf, deltaic and fluvial sediments deposited in a restricted basin. The Palaeogene sediments have a restricted macrofauna, and low diversity, with often poorly preserved microfossils that only rarely provide indications of truly marine conditions, and thus few age-diagnostic forms. Precise age constraints for certain formations of the Van Mijenfjorden Group are still controversial (Dallmann et al., 1999), but the palynological work by Manum and Throndsen (1986) has enabled assignment of a late Late Paleocene age to the Gilsonryggen Member of the Frysjaodden Formation. However the PETM had not been recognized, and it is our new stable carbon isotope, palynological and palaeomagnetic polarity data from a near-continuously exposed ~300 m succession of fine-grained clastic sediments (Fig. 2a) that now make it possible to unequivocally recognize the PETM in the Gilsonryggen Member.

Lithological logs were compiled for a Palaeogene succession SW of Longyearbyen on Nordenskiöldfjellet, starting in the sands of the Hollendardalen Formation (Dallmann et al., 1999) and extending up through the dark mudstones of the Gilsonryggen Member into the sandy Battfjellet Formation (Figs. 1d, 2). The succession was measured using a Jacob's Staff and Abney Level. The Gilsonryggen Member (here measuring ~260 m thickness) contains a conspicuous pyritic/jarositic black mudstone close to its base (at 3.5–17 m). A short interval could not be sampled (from 5.00 to 6.15 m) due to local frost heave. *In situ* samples were collected at 5-cm intervals through the lower 9.5 m of the section, and at 10-cm intervals up to 15 m; composite samples were then collected at 50-cm intervals to the top of the succession. As expected for a northern high latitude early Cenozoic succession, carbonate is virtually absent.

2.2. Palynology

Weighed samples (5–15 g) were processed using standard palynological treatment in 30% HCl, followed by decant washing and digestion in 60% HF followed by further decant washing and sieving over a 10 μm mesh. The samples were then spiked with 3–5 *Lycopodium* tablets and were brought briefly to the boil in 30% HCl and rapidly decanted into ~250 ml of water before sieving. Samples were either directly mounted using Elvacite 2044 or oxidised for ~5 min in 30% HNO_3 to remove pyrite and/or treated for 5–15 s with a tunable ultrasonic probe, followed by re-sieving to remove amorphous organic matter (AOM). Quantitative palynological data were collected by counting 300 marine palynomorphs per sample where possible (including acritarchs and simple sacs containing accumulation bodies). Samples from 0 to 4.5 m and above 13 m only yielded sparse assemblages of dinocysts, with <300 specimens per slide, making the relative abundance data in these intervals less reliable and absolute abundances have higher uncertainty. However, within the 'main body' of the PETM CIE, >300 dinocysts per slide were consistently observed, and therefore these assemblages can reliably be used to assess palaeoceanographic changes in the basin (see Discussion). *Cicatricosisporites* spores and foram test linings were counted separately from the marine palynomorphs. These data have been normalized against the out-of-count *Lycopodium* spike (Stockmarr, 1972). We employ the dinoflagellate cyst (dinocyst) taxonomy of Fensome and Williams (2004).

2.3. Organic carbon geochemistry

A total organic carbon (TOC) profile through the Gilsonryggen Member was constructed from composite samples collected at 0.5-m intervals. Fifteen grams of each homogenised sample was powdered in an agate mill, and 1 g of each sample (for TOC and $\delta^{13}C_{TOC}$ analysis) was then decarbonated in 10% Analar HCl, followed by further decarbonation in 37% Analar HCl. These samples were decant washed and oven dried at 40 °C. Isotopically analysed samples had TOC% determined using a Carlo-Erba CE-1108 elemental analyzer calibrated with Imidizole. Analytical precision is <0.2%.

Atomic H/C analyses were made with oven dried (40 °C) kerogen isolates using the elemental analyser reconfigured for N, C and H.

Carbon isotope analysis was conducted on organic carbon ($\delta^{13}C_{TOC}$). Samples were weighed to a constant C content (15 μg) before running on a Euro EA elemental analyzer linked to an Iso Prime mass spectrometer at the National Oceanography Centre, Southampton. Calibration was accomplished using a low organic carbon soil standard (EA Ltd, B2153, TOC 1.65%) with a $\delta^{13}C_{TOC}$ of −27.46‰. Analytical precision is 0.15‰.

2.4. Palaeomagnetic analyses

Sixty-six samples, from 42 horizons within the stratigraphic interval between 23 and 175 m, were subjected to progressive

Please cite this article as: Harding, I.C., et al., Sea-level and salinity fluctuations during the Paleocene–Eocene thermal maximum in Arctic Spitsbergen, Earth Planet. Sci. Lett. (2011), doi:10.1016/j.epsl.2010.12.043

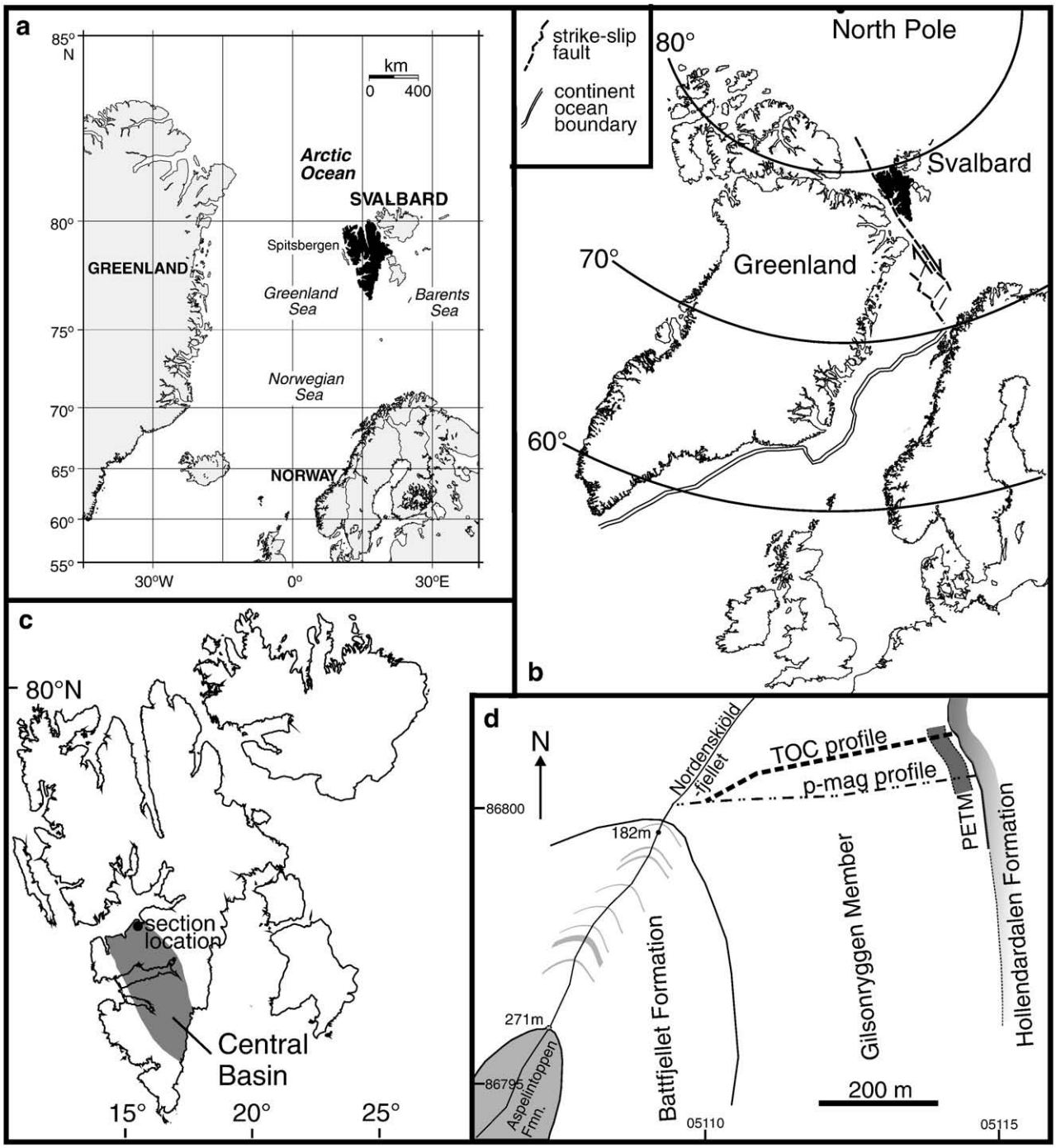

Fig. 1. Location maps of (a) Spitsbergen (black) within the Svalbard Archipelago, (b) Eocene palaeogeographic reconstruction of Spitsbergen (black; after Mosar et al. (2002)), (c) the approximate extent of the Spitsbergen Central Basin (shaded), (d) location map of the studied section (Universal Transverse Mercator grid co-ordinates), with locations of sample transects and the positions of the Hollendardalen, Battfjellet and Asplintoppen sands (light grey), and the PETM black mudstones (dark grey).

stepwise demagnetization to determine the palaeomagnetic polarity. Forty-eight of the samples were analysed using alternating field (AF) demagnetization at successive peak fields of 5, 10, 15, 20, 25, 30, 35, 40, 50, 60, 80, and 100 mT. The other 18 samples were analysed using thermal demagnetization with measurements made after heating at 80, 120, 160, 200, 240, 280, 320, 360, and 400 °C. The natural remanent magnetization (NRM) was measured using the 2-G Enterprises superconducting rock magnetometer housed within a magnetically shielded laboratory at the National Oceanography Centre, Southampton. Demagnetization data were inspected using vector component diagrams to identify stable characteristic remanent magnetization (ChRM) directions. Principal component analysis was used to identify the linear ChRM directions (Kirschvink, 1980) using data from a minimum of 3 demagnetization steps. The stably magnetized samples have relatively weak NRMs (9.4×10^{-5} to 2.53×10^{-3} A/m), and only 30 of the studied samples yielded stable ChRM directions (inconsistent results were obtained for duplicate samples from 3 horizons, so data are plotted for only 27 samples in Fig. 2a). Regardless, the samples generally have steep inclinations, which is consistent with expectation for the geomagnetic field at such high latitudes. All of the ChRM directions have reversed polarity (Fig. 2a), which indicates that present-day field overprints have been successfully removed using both AF and thermal demagnetization treatments. Dinoflagellate cyst and $\delta^{13}C$ data indicate that the studied

Please cite this article as: Harding, I.C., et al., Sea-level and salinity fluctuations during the Paleocene–Eocene thermal maximum in Arctic Spitsbergen, Earth Planet. Sci. Lett. (2011), doi:10.1016/j.epsl.2010.12.043

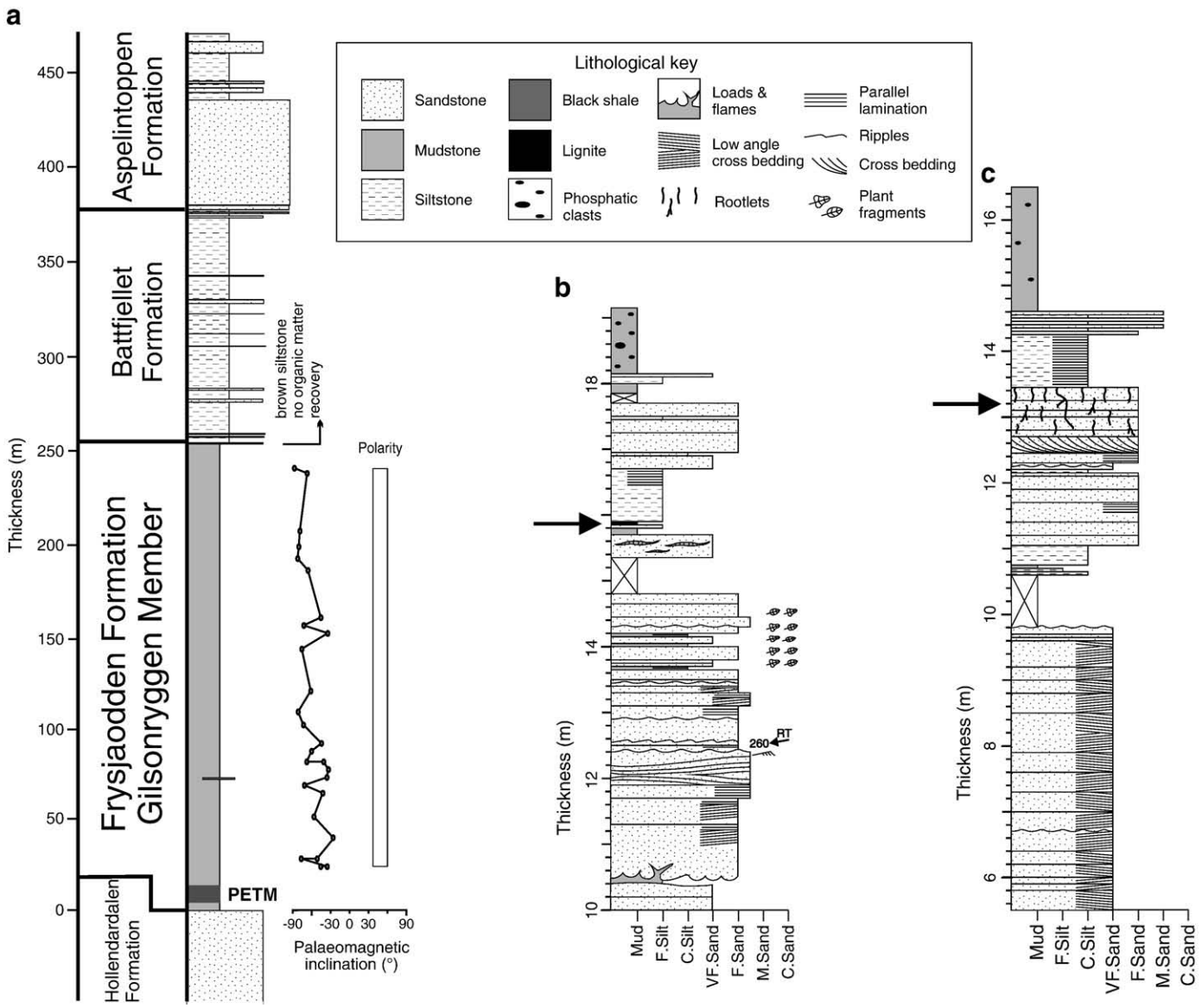

Fig. 2. (a) Measured lithological column of the studied section, indicating palaeomagnetic results for the Gilsonryggen Member. (b and c) Detailed lithological logs of the uppermost Hollendardalen Formation and lowermost Gilsonryggen Member from two measured sections (b = Locality 1; c = Locality 2) on the eastern side of Nordenskiöldfjellet. Horizontal arrows in panels b and c indicate evidence for terrestrial deposition, coals and rootlet horizons respectively.

stratigraphic interval contains the PETM, thus the thick documented interval of reversed polarity must represent the 3.1 My period of reversed polarity, Chron C24R (Westerhold et al., 2007).

2.5. Inorganic geochemical analyses

2.5.1. Bulk geochemical analyses

Bulk mineral analysis by X-ray diffraction (XRD) was undertaken on 77 samples from the 0 to 28 m interval in the Gilsonryggen Member. The <2 μm fraction of a further 8 samples was also analysed. Bulk samples were mixed with 25% by weight corundum and then ground in propan-2-ol for 8 min using a McCrone Micronizer. The ground sample was dried on a hot plate at 70 °C in a fume cupboard. The dry samples were side-loaded into an XRD sample holder and run from 2° to 70° 2θ on a Phillips XPert-Pro Powder X-ray Diffractometer System fitted with a Cu X-ray tube. Semi-quantitative analysis was achieved using a method similar to that of Chipera and Bish (2002). Detection limits are ca.0.5–1%, with precision of analyses ± 1–2% for quartz.

2.5.2. Clay mineral analysis

Samples were prepared following the methods for preparing standard <2 μm clay fractions for XRD analysis, as described by Chamley (1989). Smear slides were measured air-dried (2–15° 2θ), after ethylene glycol solvation (2–45° 2θ), and after heating to 375 °C and 550 °C (both across 2–15° 2θ). Clay proportions were calculated according to the method of Biscaye (1965). Detection limits for clays are ~2–5%, and precision of total clay and kaolinite analyses is estimated to be ± 5–10% of the amount present at percentages greater than 15% (Schultz, 1964).

3. Results

3.1. Carbon isotope excursion

A −4‰ carbon isotope excursion in bulk organic matter ($\delta^{13}C_{TOC}$; values from −26 to −30‰) occurs at the base of the Gilsonryggen Member in Spitsbergen (Fig. 3a), and coincides with the appearance of the PETM-diagnostic dinoflagellate cyst species *Apectodinium augustum*. The stable isotope and palynological data, together with the reversed

Please cite this article as: Harding, I.C., et al., Sea-level and salinity fluctuations during the Paleocene–Eocene thermal maximum in Arctic Spitsbergen, Earth Planet. Sci. Lett. (2011), doi:10.1016/j.epsl.2010.12.043

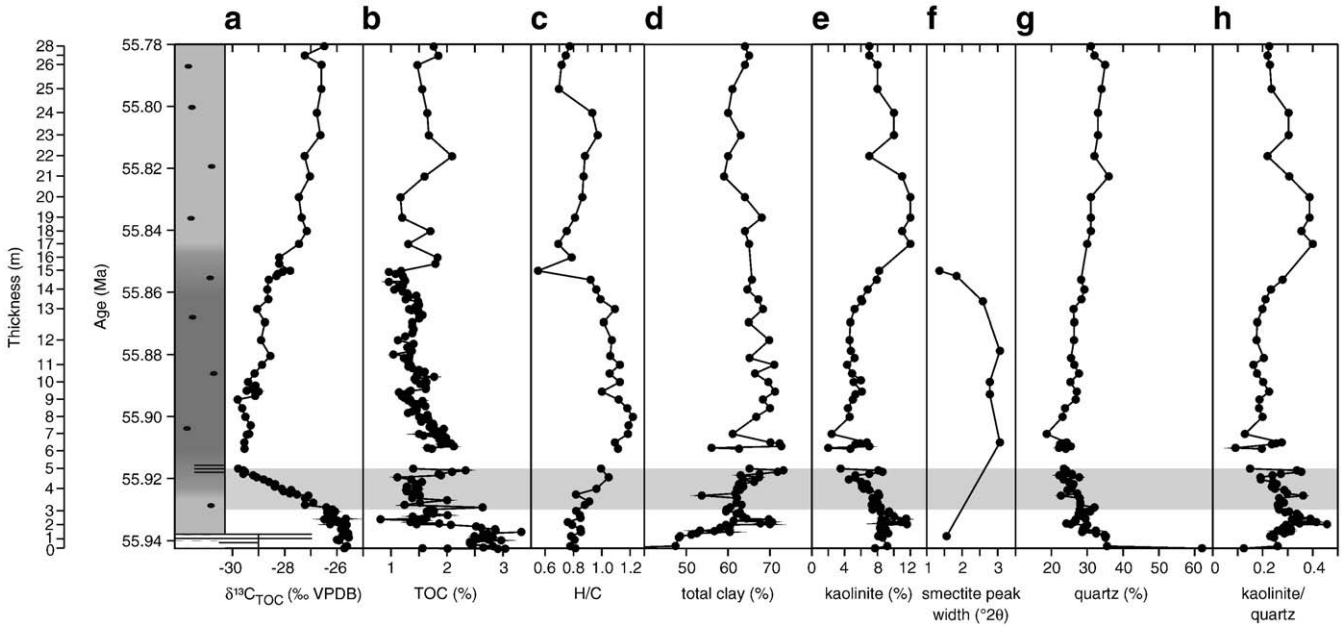

Fig. 3. Organic, geochemical and mineralogical data for the studied PETM interval, Spitsbergen. (a) $\delta^{13}C_{TOC}$ (‰ VPDB), (b) percentage TOC, (c) atomic hydrogen/carbon ratio, (d) percentage total clay, (e) kaolinite abundance, (f) smectite crystallinity, (g) quartz abundance, and (h) kaolinite/quartz ratio. Sample heights corrected to age scale (as also for Figs. 4 and 5). The grey band indicates transitional $\delta^{13}C_{TOC}$ values from the onset to the peak of the PETM CIE. See Fig. 2 for lithological key.

palaeomagnetic polarity of the Spitsbergen succession, therefore allows unequivocal recognition of the PETM within the Gilsonryggen Member. The onset of the $\delta^{13}C_{TOC}$ excursion occurs immediately prior to the lithological transition into the black mudstone. The excursion (Fig. 3a) is similar in magnitude to other PETM records from shallow marine successions (John et al., 2008; Sluijs et al., 2007b), including those measured from dispersed organic carbon (Crouch et al., 2003a,b; Magioncalda et al., 2004; Sluijs et al., 2006, 2008a; Steurbaut et al., 2003), higher plant *n*-alkanes (Pagani et al., 2006) and dinoflagellate cyst isolates (Sluijs et al., 2007b). $\delta^{13}C_{TOC}$ values from the lowermost part of the Spitsbergen succession undergo small amplitude fluctuations between −25.6 and −26.3‰. The onset of the CIE is marked by an abrupt stepwise decrease, first to −.2‰ at 3.30 m, and then to −.8‰ at 5.0 m. The amplitude of the CIE in Spitsbergen is thus ~4‰, but this may not represent the true magnitude of the excursion for two reasons: there is a sampling gap of just over 1 m (because the succession is disturbed by frost heave between 5 and 6 m), and because we analysed bulk organic carbon residues representing admixed organic carbon from a variety of sources (Handley et al., 2008; Schouten et al., 2007). Between 5 and 9 m, $\delta^{13}C_{TOC}$ values remain stable, followed by a rise of some 2.4‰ toward 17 m. Above 17 m, there is an asymptotic return to pre-excursion values toward 28 m.

We note that the shape of the onset of the Spitsbergen $\delta^{13}C_{TOC}$ excursion is atypical, with multiple transitional values between the onset and peak of the excursion, and acknowledge that these transitional values are partly the result of admixed sources of organic matter, together with the expanded sedimentation rates in this foreland setting. Pre-Palaeogene reworking of organic matter has not appreciably affected the Spitsbergen TOC or $\delta^{13}C_{TOC}$ records, as the reworked Palaeozoic and Mesozoic palynomorphs are extremely rare throughout the Gilsonryggen Member. A comparison of $\delta^{13}C_{TOC}$ data and compound specific carbon isotopes ($\delta^{13}C_{n\text{-alkane}}$) from a second PETM succession in Spitsbergen indicates that the inflection points of the PETM CIE in both $\delta^{13}C_{TOC}$ and $\delta^{13}C_{n\text{-alkane}}$ were coeval (Cui, 2010), validating the use of the Longyearbyen $\delta^{13}C_{TOC}$ curve as an external constraint on our age model (Section 3.2; Supplementary Material). Furthermore, the presence of 5 cycles within the 'main body' of the PETM CIE in the depth domain of the Longyearbyen section and ODP sites 690 and 1263 (Röhl et al., 2007), illustrates this interval of the Spitsbergen succession is complete and lacking hiatuses of any significance (Fig. S1).

3.2. Age model

A chronology for the Spitsbergen succession has been developed using palaeomagnetic, chemo- ($\delta^{13}C_{TOC}$, Figs. 3a, S3b; and total organic carbon (TOC) analysis: Fig. S3a), bio- and cyclo-stratigraphy. The $\delta^{13}C_{TOC}$ PETM excursion has been matched to the bulk carbonate CIE record from ODP Site 1263 (age model of Röhl et al., 2007) to constrain the age of the lowermost part of the Spitsbergen succession. It has thus been possible to determine relative sedimentation rates between the onset of the excursion at around 3 m to the end of the 'main body' of the PETM CIE (as defined by Röhl et al., 2007) which average 17.4 cm/kyr (Fig. S4; range = 8.7 to 23.4 cm/kyr). This is about an order of magnitude higher than most deep marine sections, and similar to rates derived for continental margin successions from New Jersey and California (John et al., 2008). However, we note a minor hiatus is present at the onset of the PETM at Site 1263 due to carbonate dissolution (e.g. Zachos et al., 2005), and thus the duration of the onset of the PETM in our age model will be slightly underestimated. Orbitally forced variations in TOC from Spitsbergen (Fig. S2) were then tuned using previous estimates of the relative duration of Chron 24R based on the high quality cyclical Fe record (Fig. S3c, d) from Site 1263 (Westerhold et al., 2007; corrected after Röhl et al., 2007) to obtain an age model for the studied succession. The numerical ages adhere to age Option 2 of Westerhold et al. (2007) but may be shifted by ±400 kyr (see Supplementary Material). We note that no precise independent constraints on the age model for the post-PETM interval are available, and therefore the ages derived for the post-PETM interval carry greater uncertainty.

However, for the interval between the PETM and the top of the Gilsonryggen Member, cyclical TOC variations have a strong orbital obliquity (~41 kyr) and precession (~21 kyr) signal (both before and after tuning), which suggests an average sedimentation rate of around 22 cm/kyr (Fig. S4; range 12.5 to 34.4 cm/kyr) for the post-PETM interval up to the top of the unit. It was not possible to establish a sedimentation rate for the short pre-PETM section. By interpreting the observed ratios of periods in the data with orbital templates (Fig. S2;

Please cite this article as: Harding, I.C., et al., Sea-level and salinity fluctuations during the Paleocene–Eocene thermal maximum in Arctic Spitsbergen, Earth Planet. Sci. Lett. (2011), doi:10.1016/j.epsl.2010.12.043

Pälike et al., 2008; Raffi et al., 2005), an average sedimentation rate of 12–22 cm/kyr can be determined, the upper end of this estimate being similar to and consistent with the rates established above.

3.3. Organic matter abundance and characteristics

Many PETM records contain elevated organic carbon concentrations (Crouch et al., 2003b; John et al., 2008), including those from the Arctic (Sluijs et al., 2006, 2008a; Stein et al., 2006), New Jersey (John et al., 2008; Zachos et al., 2006), California (John et al., 2008), and the Tethys (Bolle et al., 2000; Crouch et al., 2003b; Gavrilov et al., 2003). In contrast, TOC levels in Spitsbergen (Fig. 3b) are higher before the PETM (~3%) and decrease (~1.5%) a metre below the onset of the hyperthermal, and remain at this lower level throughout the main body of the PETM. TOC does not return to pre-PETM levels in the remainder of the ~180 m of studied section. However, given the relatively high PETM sedimentation rates (~17 cm/kyr) compared to other localities, TOC values of ~1.5% suggest that the Spitsbergen Central Basin would have been a significant carbon sink during the PETM (Charles et al., in preparation).

Pre- and post-CIE sediments are characterized by palynofacies dominated by terrestrially derived phytoclasts (i.e., cuticle and 'wood', a small fraction of which are possibly reworked, as at Site 302-4A; see Stein et al., 2006), and low abundances of *in situ* marine plankton and amorphous organic matter (AOM). This contrasts with the CIE, which is characterized by a high abundance of AOM and marine plankton, but very subordinate terrestrially derived phytoclasts. This 'switch' from phytoclast-dominated to AOM-dominated palynofacies is confirmed by the systematic increase of the atomic H/C ratio in bulk organic matter into the 'main body' of the CIE in Spitsbergen (Fig. 3c). Given that the AOM is granular, clotted ('grumose': Tyson, 1995), contains rare marine inclusions (e.g. dinocysts), has the fluorescence properties of marine AOM, and dominates the palynodebris isolated from the reducing conditions of the 'main body' of the CIE (see Section 4.1), it is likely to be dominantly of marine origin (Batten, 1983; Tyson, 1995, p.249).

3.4. Palynomorph assemblages

Below the studied PETM interval, terrestrially dominated palynofacies are characterized by phytoclasts of brown wood and cuticle with extremely low abundances of *in situ* marine dinocysts, which are almost exclusively *Spiniferites* spp. (Figs. 4 and 5). The transition into the PETM is characterized by a large increase in marine dinocyst abundance and diversity (Fig. 4), as is the case at Site 302-4A (Sluijs et al., 2006, 2008a). There is also a conspicuous abundance peak in large *Cicatricosisporites* spp. fern spores at the base of the PETM (acme ~5 kyr after onset CIE), the number and restricted occurrence of which argues against reworking of Cretaceous forms (Fig. 4i).

In common with results from other sites, the PETM is characterized by the appearance of the dinocyst genus *Apectodinium* (reaching concentrations of >26,000 cysts/g; Figs. 4b and 5b), and is dominated by *A. augustum*. However, while *Apectodinium* is found in flood abundance, it is numerically subordinate to another peridinioid dinocyst, *Senegalinium obscurum*, which can exceed concentrations of 150,000 cysts/g (Figs. 4c and 5c). There is a striking co-dominance of these two dinocysts throughout the PETM interval. Increased dinocyst diversity is represented by the appearance of peridinioids *Spinidinium*/*Lentinia* (Figs. 4e and 5e), *Cerodinium*/*Deflandrea* (Fig. 4f) and *Palaeocystodinium*, but *Cerodinium*/*Deflandrea* is never a major component of assemblages in the lower part of the PETM as it is at Site 302-4A (Fig. 5f; Sluijs et al., 2008a). However, the Spitsbergen succession has not only a lower dinocyst species diversity than that at Site 302-4A but it is also lower than in many other PETM records (e.g., Crouch and Brinkhuis, 2005; Crouch et al., 2003b; Powell et al., 1996; Sluijs and Brinkhuis, 2009). In contrast to the Site 302-4A record, the fully marine gonyaulacoid genera *Glaphyrocysta*/*Areoligera* (Figs. 4g and 5g), *Diphyes*, *Hystrichokolpoma*, *Lanternosphaeridium* and *Muratodinium* are most abundant within the main body of the CIE excursion, not toward its termination. Also, unlike PETM successions in which a benthic foraminiferal extinction event is recorded, organic-walled test linings of benthic foraminifera first appear within the main CIE interval, and after a brief absence are again found after the CIE (Fig. 4h).

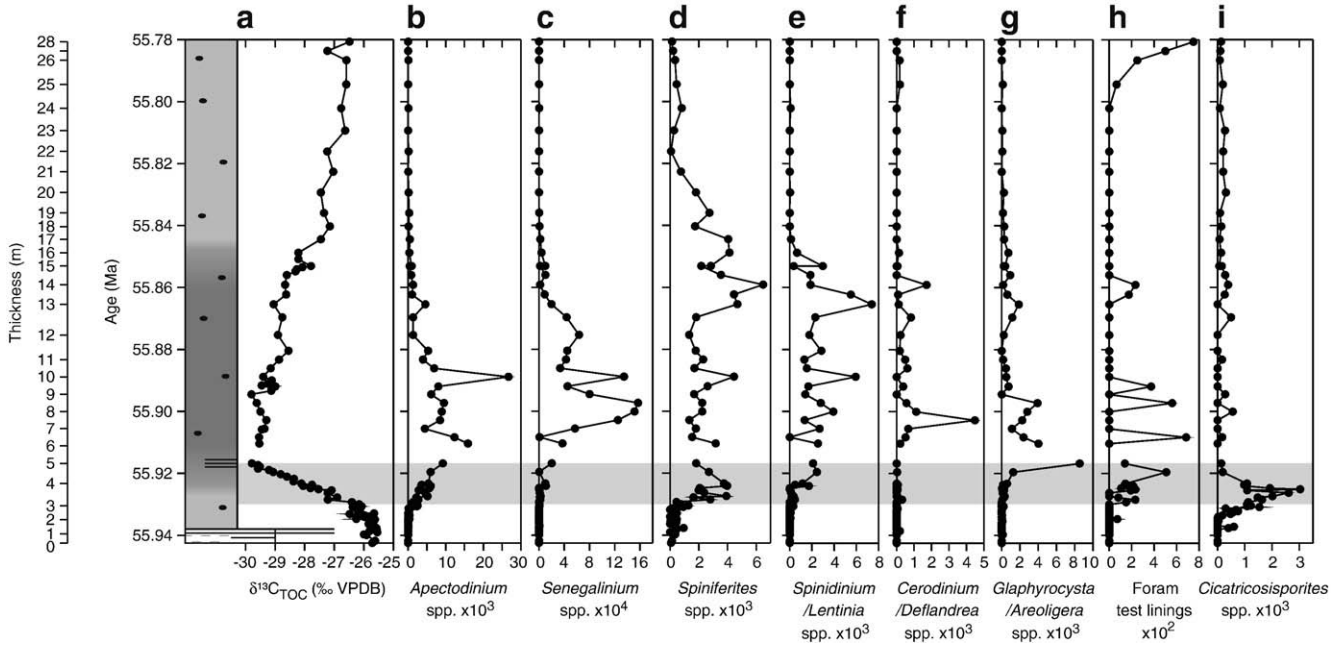

Fig. 4. Abundances of selected palynomorphs from the lower part of the Gilsonryggen Member, plotted against the $\delta^{13}C_{TOC}$ curve. The grey band indicates transitional $\delta^{13}C_{TOC}$ values from the onset to the peak of the PETM CIE. Note the different scales for palynomorph absolute abundances. See Fig. 2 for lithological key.

Please cite this article as: Harding, I.C., et al., Sea-level and salinity fluctuations during the Paleocene–Eocene thermal maximum in Arctic Spitsbergen, Earth Planet. Sci. Lett. (2011), doi:10.1016/j.epsl.2010.12.043

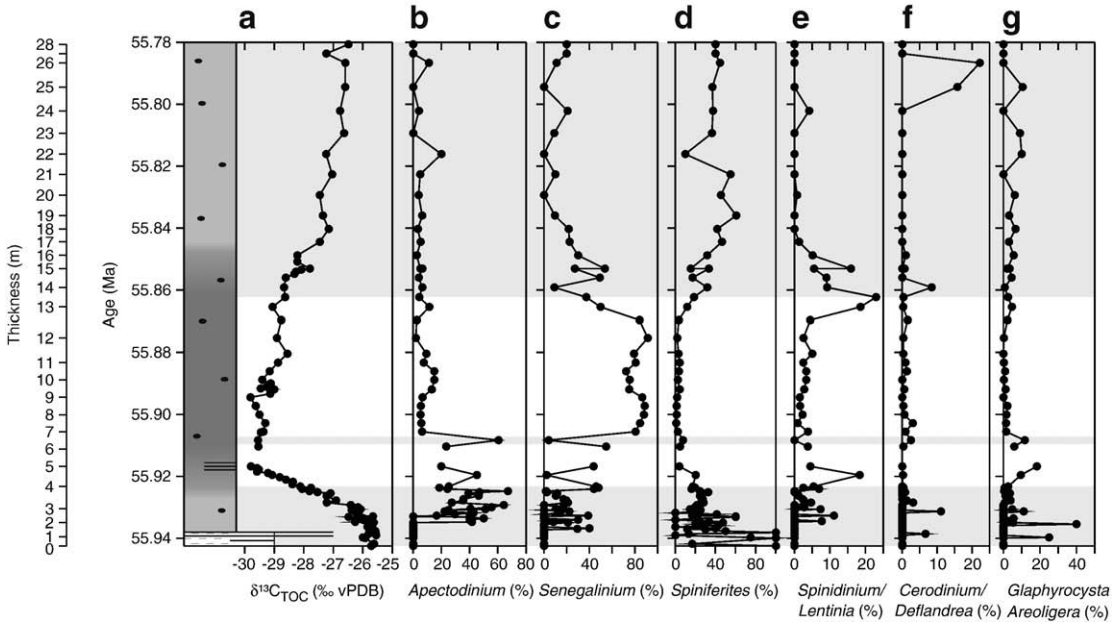

Fig. 5. Relative abundances of selected dinocyst taxa from the lower part of the Gilsonryggen Member, plotted against the $\delta^{13}C_{TOC}$ curve. Grey bars indicate samples where <300 dinocysts were counted, and relative abundances are less precise. See Fig. 2 for lithological key.

3.5. Clay and other minerals

Kaolinite, quartz (Fig. 3e, g), plagioclase feldspar and the kaolinite/quartz (K/Q) ratio (Fig. 3h) decrease commensurate with increases in total clay content (Fig. 3d). The initial decline in quartz and feldspar occurs at a stratigraphic height of ~1.5 m, compared to ~3 m for kaolinite. Quartz and plagioclase contents remain essentially unchanged between 5 and 9 m, at which point they progressively increase up to 17 m. Half-height peak width measurements of the 001 smectite peak (Fig. 3f) have values less than 1.6° (2θ) above and below the excursion, and greater than 2.5° within the CIE. Smectite abundance also increases within the excursion. The decline in kaolinite within the CIE contrasts with increased kaolinite abundance in other PETM records, e.g., North America (Gibson et al., 1993, 2000) and the South Atlantic and Southern Ocean (Robert and Chamley, 1991; Robert and Kennett, 1994).

4. Discussion

We have presented results from the highest-resolution Arctic PETM record to date, which permits comparisons with the data from Arctic Site 302-4A and elsewhere.

4.1. Water column oxygenation

At Site 302-4A the photic zone became, at least intermittently, anoxic, as indicated by the presence of isorenieratene, a biomarker derived from photosynthetic green sulphur bacteria and the absence of foram test linings (Sluijs et al., 2006, 2008a). Laminated sediments, elevated organic carbon and C/S ratios (Sluijs et al., 2008a; Stein et al., 2006) all indicate anoxic conditions. Development of low oxygen conditions during the PETM in Spitsbergen is also indicated by increased abundances of more labile organic matter (AOM vs. phytoclasts) and the lowest Th/U values of the entire Gilsonryggen Member (Dypvik et al., in press). However, despite the presence of sedimentary laminations at the CIE peak, the dark Spitsbergen mudstones also contain benthic foraminiferal test linings. The extremely small numbers of these specimens might be interpreted as either representing very minor reworking of older material (numbers of specimens being similar to the small numbers of reworked dinocysts), or Eocene specimens transported from more proximal areas of the basin. Abundance and diversity parameters for these agglutinated assemblages reach their minimum values for the entire Spitsbergen Palaeogene through the PETM, indicating the most highly stressed environmental conditions: the very sparse PETM assemblages are dominated by single species of *Trochammina* and *Thurammina* (Nagy, *pers. comm.*). This is compatible with sedimentological and geochemical data which indicate low bottom water oxygenation prevailed during the CIE, and thus the test linings may represent brief (perhaps seasonal) periods with elevated oxygen conditions when stress-tolerant (poikiloaerobic) forams were able to colonize the seafloor in low numbers — akin to the situation known from the Kimmeridge Clay (Jenkins, 2000). Thus, although low oxygen bottom water conditions prevailed as a result of raised temperatures, water column stratification and the restricted basinal setting of the Gilsonryggen Member, the more weakly developed sedimentary lamination suggest that this part of the Central Basin did not experience anoxia extending into the photic zone as experienced at Site 302-4a during this hyperthermal event.

4.2. Salinity and runoff

Fluctuations in salinity and terrestrial runoff across the PETM have been documented for neritic localities in New Jersey (Gibson et al., 2000; John et al., 2008; Zachos et al., 2006) and New Zealand (Crouch et al., 2003a), in addition to Site 302-4A (Pagani et al., 2006; Sluijs et al., 2006, 2008a; Waddell and Moore, 2008). Similar evidence exists during the PETM in Spitsbergen. Both prior to, and after, deposition of the dark PETM mudstones, palynological evidence indicates low salinities compared to normal marine waters in the restricted Central Basin (i.e. extremely low abundance of refractory marine dinoflagellate cysts and dominantly terrestrially derived phytoclasts). The abundance of terrestrial organic matter is also higher before and after the CIE at Site 302-4A (Sluijs et al., 2006; Weller and Stein, 2008).

More normal marine salinities developed within the Central Basin during the CIE, as demonstrated by higher diversity, fully marine dinocyst assemblages (Section 3.4). There are indications that the water column became stratified (sediment lamination, pyrite and AOM abundances, *Senegalinium* abundances), with more normal marine deeper waters being overlain by a freshened surface lens

Please cite this article as: Harding, I.C., et al., Sea-level and salinity fluctuations during the Paleocene–Eocene thermal maximum in Arctic Spitsbergen, Earth Planet. Sci. Lett. (2011), doi:10.1016/j.epsl.2010.12.043

resulting from elevated terrestrial run-off. This interpretation is supported by the incoming of flood abundances of *Senegalinium obscurum* (Figs. 4c and 5c), a peridinioid species often found in association with low diversity, high dominance, low salinity dinocyst assemblages and freshwater chlorococcalean algae (e.g., *Pediastrum, Botryococcus*: Sluijs and Brinkhuis, 2009; Sluijs et al., 2006, 2008a). The abundance increases in *S. obscurum* through the CIE (33 and ~41 kyrs after the onset) may suggest successive pulses of increased run-off into the Central Basin. Furthermore, the dramatic increase in the abundances of terrestrially derived *Cicatricosisporites* fern spores (~5 kyrs after the onset of the excursion: Fig. 4i) may represent another such pulse, although we acknowledge that this could also be an ecologically-induced signal.

Relative and absolute abundances of *Senegalinium obscurum* reach a peak 33 kyr after the onset of the PETM, resulting in near-monospecific assemblages dominated by this taxon. This suggests water column stratification reached a peak 33 kyr after the initiation of the hyperthermal event. These results are again consistent with those from Site 302-4A, where high runoff low-salinity conditions have also been inferred from the persistent dominance of low salinity dinocyst taxa (Sluijs et al., 2008a) and $\delta^{18}O$ analyses of fish bones (Waddell and Moore, 2008), although the Spitsbergen palynological data are quantitatively different to those from Site 302-4A. Thus, several lines of evidence support increased atmospheric moisture transport (manifested as elevated run-off) to the high Arctic during the PETM in response to global warming (Pagani et al., 2006).

Angiosperm pollen is exceedingly rare throughout the studied section and even during the PETM it is an exceedingly minor component. This is in stark contrast to Site 302-4A (Sluijs et al., 2006, 2008a), in which angiosperm pollen forms a significant component of the palynomorph assemblages, and other sites which indicate an increase in angiosperm over gymnosperm communities during the PETM (e.g. Smith et al., 2007). This may have been in part due to any (small) angiosperm pollen being deposited further offshore or alternatively Spitsbergen had fewer flowering plants in the hinterland. The near-absence of angiosperm pollen at other more distal Central Basin sites (Charles, pers. obs.) may indeed indicate that conditions around the Spitsbergen Central Basin were not optimal for angiosperm growth during the PETM.

4.3. Mineralogical interpretations

Elevated kaolinite abundance has been used as a proxy for increased chemical weathering in temperate and southern hemisphere high-latitude PETM successions associated with increased rainfall under higher temperature conditions (Gibson et al., 1993; Robert and Chamley, 1991; Robert and Kennett, 1992, 1994). At Spitsbergen, increased kaolinite supply would be expected to raise the kaolinite/quartz (silt) ratio. Alternatively, if the origin of the two minerals is linked, the ratio would remain constant. A decline in this ratio could result from a reduction in the elevation of the hinterland being eroded, which is unlikely in this foreland basin, or from an increasingly distal depositional setting. Kaolinite abundance is reduced more than quartz silt during the PETM (Fig. 3g), and although fluctuations are relatively minor, the relative variations may be explained by increased distance from source resulting in differential settling of kaolinite particles, as is the case for settings offshore from the Amazon (Gibbs, 1977).

Smectite crystallinity is elevated during the CIE (Fig. 3f). As noted by Chamley (1989), smectite crystallinity can incorporate a contribution from irregular mixed-layers, which tend to increase in abundance with increasing hydrolysis in temperate climate regimes. Increased regional precipitation and thus intensified hydrolysis of clay assemblages at source may have produced the expansion of the smectite 001 peak, however we cannot rule out a change in sediment source.

4.4. Changes in relative sea level

By integrating palynological and geochemical data with sedimentological evidence from Spitsbergen, it is possible to reconstruct relative sea level changes across the PETM. The hyperthermal event is recorded within the mudstone-dominated Gilsonryggen Member, which lies immediately above the sandstone-dominated deltaic Hollenderdalen Formation. The top of the latter unit contains a 5–10 cm-thick lignite seam at Locality 1 (arrow in Fig. 2b) and a series of rootlet horizons are developed in thin sands at Locality 2 (arrow in Fig. 2c). The top of the Hollendardalen Formation therefore represents an emergent terrestrial environment. The onset of mudstone deposition with low diversity marine dinocyst assemblages in the basal Gilsonryggen Member is therefore indicative of a marine transgression, which occurred before the onset of the PETM CIE. Continued reduction in quartz and plagioclase feldspar percentages up-section indicates an increasingly distal sediment source throughout the event, which implies that sea level continued to rise before the onset of the PETM. Establishment of more normal marine salinities was coincident with the CIE, as evidenced both by higher diversity, fully marine dinocyst assemblages (e.g. increases in *Glaphyrocysta*/*Areoligera* abundance — Figs. 4g and 5g: Powell et al., 1996; Sluijs and Brinkhuis, 2009), and by increased abundances of taxa associated with more distal settings, such as *Spiniferites* (Fig. 4d: Brinkhuis, 1994; Sluijs et al., 2008b). Marine salinities may also be corroborated by the appearance of test linings of agglutinated foraminifera during the peak CIE (Fig. 4h), and more distal settings by decreases in the abundances of terrestrially derived phytoclasts and large spores, which are coeval with the development of sedimentary laminations (Fig. 6). Still lower quartz silt content in the finer-grained black PETM mudstones provide further evidence for an increasingly distal setting, which is comparable with the findings of John et al. (2008) and Miller et al. (1998) in New Jersey. Therefore, both palynological and geochemical evidence suggest that maximum sea levels were recorded at the peak of the PETM CIE, ~13 kyr after the onset of the excursion.

Although small numbers of foraminiferal test linings are found during the later stages of the CIE recovery, most distal marine indicators become less common: dinocyst diversities become lower and phytoclasts also return to dominate the palynofacies, which indicate increasing proximity to the terrestrial source. There is therefore strong evidence that the Hollenderdalen Formation/Gilsonryggen Member boundary represents an initial flooding surface. Above this boundary, the basal Gilsonryggen Member consists of mudstones deposited during a marine transgression (with deepening and increasing distance from shore), with a maximum flooding surface (MFS) developed at the CIE peak.

4.5. Relative verses eustatic sea level rise

Fluctuations in relative sea level during the PETM have been described from the Atlantic (Cramer et al., 1999; Gibson et al., 1993; John et al., 2008; Sluijs et al., 2008b), Pacific (Crouch and Brinkhuis, 2005; John et al., 2008; Sluijs et al., 2008b), Tethyan (Gavrilov et al., 2003; Speijer and Morsi, 2002; Speijer and Wagner, 2002) and Arctic Oceans (Sluijs et al., 2006, 2008a), and the Turgay Strait (Iakovleva et al., 2001). A summary of the sedimentological, geochemical and biotic proxies used to infer these relative sea level changes is provided in Table S1. This relative sea level rise has been correlated with the North Sea Thanetian 5 sequence (Bujak and Brinkhuis, 1998; Hardenbol, 1994; Powell et al., 1996) by Sluijs et al. (2008b), who renamed it the Ypresian 1 sequence, because of more recent downward revision of the Paleocene–Eocene boundary. Taken together, these records indicate a eustatic sea level rise at the Paleocene–Eocene boundary, with evidence from the New Jersey

Please cite this article as: Harding, I.C., et al., Sea-level and salinity fluctuations during the Paleocene–Eocene thermal maximum in Arctic Spitsbergen, Earth Planet. Sci. Lett. (2011), doi:10.1016/j.epsl.2010.12.043

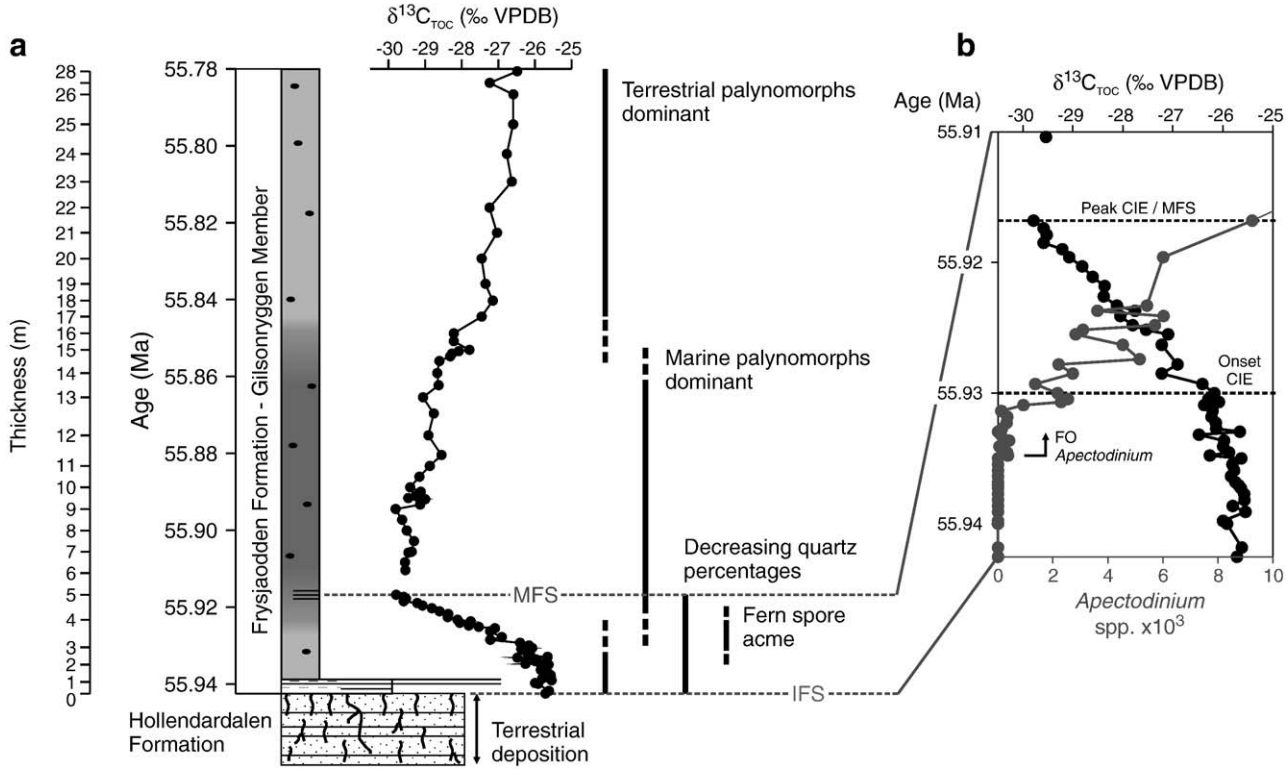

Fig. 6. Summary diagram of key features of the PETM in Spitsbergen. (a) Selected sedimentological, geochemical and palynological changes plotted against $\delta^{13}C_{TOC}$. IFS = initial flooding surface, MFS = maximum flooding surface. See Fig. 2 for lithological key. (b) Expanded view of the stratigraphic interval between the IFS and MFS, indicating the first occurrence (FO) of *Apectodinium* relative to the PETM CIE.

margin suggesting that the onset of sea level rise preceded the PETM by 20–200 kyr (Sluijs et al., 2008b).

Although the burial history of the Spitsbergen Central Basin is not sufficiently resolved to disentangle the effects of orogenic loading from eustatic change (see Blythe and Kleinspehn, 1998 for burial history), development of a maximum flooding surface (MFS) at the peak of the PETM CIE indicates that this surface is exactly coeval with other high resolution records of PETM sea level rise. Thus, the Spitsbergen sea level rise can be taken to represent a eustatic change that overprinted other more localised factors (e.g., tectonic subsidence, sediment supply rate). The Spitsbergen data provides further evidence to substantiate the contention that the onset of eustatic rise preceded the CIE (Sluijs et al., 2008b). Thermal expansion of seawater, melting from small-scale Antarctic alpine glaciers and/or a decrease in ocean basin volume (caused by tectonics/volcanism associated with the North Atlantic Igneous Province) have been proposed as mechanisms that could account for the pre-CIE sea level rise (Sluijs et al., 2008b).

4.6. *Apectodinium* as a proxy for environmental change

The poleward migration and globally synchronous acme of the dinocyst genus *Apectodinium* (including PETM-marker *A. augustum*) is unique in the entire (Mid Triassic–Holocene) dinocyst record (Crouch et al., 2001; Sluijs and Brinkhuis, 2009). Furthermore the appearance of *Apectodinium* before the CIE in several localities has been taken as evidence for the onset of environmental change prior to the isotopic perturbation of the ocean–atmosphere system (Sluijs et al., 2007b). However, several environmental factors have been implicated to explain the spatial distribution of this taxon, including elevated (possibly seasonal) supply of terrestrially derived nutrients (Bujak and Brinkhuis, 1998; Sluijs et al., 2006), in New Jersey (Sluijs and Brinkhuis, 2009), New Zealand (Crouch and Brinkhuis, 2005), Tunisia, Uzbekistan (Crouch et al., 2003b) and at Site 302-4A (Sluijs et al., 2006, 2008a). In Spitsbergen, the highest abundances of *Apectodinium* also occur during peak runoff, and thus by inference when delivery of terrestrially derived nutrients was also at a maximum (see Section 4.2).

Sea surface temperature (SST) also appears to have been a significant controlling factor in the distribution of this genus, which was restricted to low latitudes until it migrated poleward with rising SSTs (Brinkhuis et al., 1994; Bujak and Brinkhuis, 1998; Crouch et al., 2003b; Sluijs and Brinkhuis, 2009). Although canonical correspondence analysis of the New Jersey margin dinoflagellate cyst assemblages provides corroboration of the link between *Apectodinium* abundances and elevated SSTs, temperature was not the only limiting ecological factor on its distribution (Sluijs and Brinkhuis, 2009).

The first occurrence of the genus in the Spitsbergen succession occurs around 1.05 m below the onset of the PETM CIE (Fig. 6), and it is consistently present in low abundance (over 100 specimens from 12 out of 13 samples) before the onset of the event. Although the genus has been observed in the stratigraphically lower Grumantbyen Formation, (Manum and Throndsen, 1986), the number of pre-CIE specimens and extremely low abundance of reworked palynomorphs (<200 cysts g^{-1}) in this interval implies the records are not an artefact of reworking. Furthermore, given the pyrite concentrations and the absence of visible burrows through the 1.05 m interval in which *Apectodinium* occurs, the low oxygen conditions suggests that bioturbation was not responsible for its pre-CIE record. The Longyearbyen record of *Apectodinium* thus not only implies that the minimum temperature tolerances for this taxon had been reached, but that environmental change in the Arctic had begun prior to the CIE.

5. Conclusions

The Gilsonryggen Member of the Frysjaodden Formation in Spitsbergen records a negative $\delta^{13}C_{TOC}$ excursion of ~4‰ in a clay–silt succession with reversed magnetic polarity that is accompanied by an acme of the dinocyst genus *Apectodinium*. The presence of *A. augustum* during the CIE allows unequivocal identification of the

Please cite this article as: Harding, I.C., et al., Sea-level and salinity fluctuations during the Paleocene–Eocene thermal maximum in Arctic Spitsbergen, Earth Planet. Sci. Lett. (2011), doi:10.1016/j.epsl.2010.12.043

PETM in Spitsbergen for the first time, and provides a second Arctic record of the event, in a continental margin setting deposited at a palaeolatitude of 75 °N. TOC data have been shown to demonstrate orbital cyclicities that have been used to develop an age model for the succession. Anoxic conditions did not extend into the photic zone. The organic material in the Spitsbergen pre- and post-PETM sediments is dominated by terrestrially-derived phytoclasts, with AOM and dinocysts dominating the PETM. The Spitsbergen sediments contain virtually no angiosperm pollen, in contrast to Site 302-4A, which may indicate major regional differences in Arctic basin-margin vegetation cover. By combining sedimentological and palynological evidence it has been possible to demonstrate the first evidence for sea level rise before the PETM CIE in Arctic Spitsbergen, culminating in maximum flooding during the CIE peak. High resolution biostratigraphic analysis indicates that *Apectodinium* (including *Apectodinium augustum*) appears before the onset of the carbon isotope excursion (CIE), and thus confirms the onset of environmental change in the Arctic had begun prior to the CIE. The Spitsbergen PETM succession records water column stratification during the CIE, with a low salinity surface lens above normal marine salinity waters; successive abundance peaks of *Cicatricosisporites* spores and *Senegalinium* dinocysts may corroborate predictions of an intensified hydrological cycle (e.g. Pagani et al., 2006), with maximum stratification reached 33 kyrs after the onset of the CIE. The greatly expanded succession thus indicates that the Central Basin of Spitsbergen offers much potential for conducting further high-resolution analyses of the PETM.

Supplementary materials related to this article can be found online at doi:10.1016/j.epsl.2010.12.043.

Acknowledgements

We thank Mike Bolshaw and Ross Williams for help with sample preparation and analysis, Gary Nichols for significant advice on Spitsbergen during the initial field season, and the Millennium Atlas Company Limited for funding our preliminary fieldwork. We would also like to extend our thanks to Steve Bohaty for many helpful discussions, and Appy Sluijs for his constructive review, both of which have greatly improved the final paper.

References

Abdul Aziz, H., Hilgen, F.J., Van Luijk, G.M., Sluijs, A., Kraus, M.J., Pares, J.M., Gingerich, P.D., 2008. Astronomical climate control on the paleosol stacking patterns in the upper Paleocene–lower Eocene Willwood Formation, Bighorn Basin, Wyoming. Geology 36, 531–534.

Batten, D.J., 1983. Identification of Amorphous Sedimentary Organic Matter by Transmitted Light Microscopy. In: Brooks, J. (Ed.), Petroleum Geochemistry and Exploration of Europe. : Geol. Soc. Spec. Pub., vol. 12. The Geological Society/ Blackwell, Oxford, pp. 275–288.

Bice, K.L., Arthur, M.A., Marincovich Jr., L., 1996. Late Palaeocene Arctic Ocean shallow-marine temperatures from mollusk stable isotopes. Paleoceanography 11, 241–249.

Biscaye, P.E., 1965. Mineralogy and sedimentation of Atlantic and Antarctic Ocean deep-sea sediments. Geol. Soc. Am. Bull. 76, 803–831.

Blythe, A.E., Kleinspehn, K.L., 1998. Tectonically versus climatically driven Cenozoic exhumation of the Eurasian plate margin, Svalbard: fission track analyses. Tectonics 17, 621–639.

Bolle, M.–.P., Pardo, A., Hinrichs, K.–.U., Adatte, T., Von Salis, K., Burns, S., Keller, G., Muzylev, N., 2000. The Palaeocene–Eocene transition in the marginal northeastern Tethys (Kazakhstan and Uzbekistan). Int. J. Earth Sci. 89, 390–414.

Bowen, G.J., Beerling, D.J., Koch, P.L., Zachos, J.C., Quattlebaum, T., 2004. A humid climate state during the Palaeocene/Eocene thermal maximum. Nature 432, 495–499.

Bowen, G.J., Koch, P.L., Gingerich, P.D., Norris, R.D., Bains, S., Corfield, R.M., 2001. Refined Isotope Stratigraphy across the Continental Palaeocene–Eocene Boundary on Polecat Bench in the Northern Bighorn Basin. In: Gingerich, P.D. (Ed.), Palaeocene–Eocene Stratigraphy and Biotic Change in the Bighorn and Clarks Fork Basins, Wyoming, vol. 33. Univ. Michigan Papers on Paleontology, pp. 73–88.

Bowen, G.J., Clyde, W.C., Koch, P.L., Ting, S., Alroy, J., Tsubamoto, T., Wang, Y., 2002. Mammalian dispersal at the Palaeocene/Eocene boundary. Science 295, 2062–2065.

Brinkhuis, H., 1994. Late Eocene to early Oligocene dinoflagellate cysts from the Priabonian tye area (northeast Italy); biostratigraphy and palaeoenvironmental interpretation. Palaeogeogr. Palaeoclimatol. Palaeoecol. 107, 121–163.

Brinkhuis, H., Romein, A.J.T., Smit, J., Zachariasse, W.J., 1994. Danian-Selandian dinoflagellate cysts from lower latitudes with special reference to the El Kef section, NW Tunisia. Geol. Fören. Stockh. Förh. 116, 46–48.

Bruhn, R., Steel, R., 2003. High-resolution sequence stratigraphy of a clastic foredeep succession (Paleocene, Spitsbergen): an example of peripheral-bulge-controlled depositional architecture. J. Sediment. Res. 73, 745–755.

Bujak, J., Brinkhuis, H., 1998. Global Warming and Dinocyst Changes across the Palaeocene/Eocene Epoch Boundary. In: Aubry, M.-P., Lucas, S.G., Berggren, W.A. (Eds.), Late Palaeocene–Early Eocene Biotic and Climatic Events in Marine and Terrestrial Records. Columbia Univ. Press, New York, pp. 277–295.

Chamley, H., 1989. Clay Sedimentology. Springer-Verlag, New York. pp. 623.

Charles, A., Harding, I.C., Marshall, J.E.A., Pancost, R., in preparation. High carbon burial rates during the Paleocene-Eocene Thermal Maximum in Arctic Spitsbergen. for Geology.

Chipera, S.J., Bish, D.L., 2002. FULLPAT: a full pattern quantitative analysis program for X-ray powder diffraction using measured and calculated patterns. J. Appl. Crystallogr. 35, 744–749.

Cramer, B.S., Aubry, M., Miller, K.G., Olsson, R.K., Wright, J.D., Kent, D.V., 1999. An exceptional chronologic, isotopic, and clay mineralogic record of the latest Paleocene thermal maximum, Bass River, NJ, ODP 174AX. Bull. Soc. Géol. Fr. 170, 883–897.

Crouch, E.M., Brinkhuis, H., 2005. Environmental change across the Paleocene–Eocene transition from eastern New Zealand: a marine palynological approach. Mar. Micropaleontol. 56, 138–160.

Crouch, E.M., Heilmann-Clausen, C., Brinkhuis, H., Morgans, H.E.G., Rogers, K.M., Egger, H., Schmitz, B., 2001. Global dinoflagellate event associated with the late Paleocene Thermal Maximum. Geology 29, 315–318.

Crouch, E.M., Dickens, G.R., Brinkhuis, H., Aubry, M., Hollis, C.J., Rogers, K.M., Visscher, H., 2003a. The *Apectodinium* acme and terrestrial discharge during the Paleocene–Eocene Thermal Maximum: new palynological, geochemical and calcareous nannoplankton observations at Tawanui, New Zealand. Palaeogeogr. Palaeoclimatol. Palaeoecol. 194, 387–403.

Crouch, E.M., Brinkhuis, H., Visscher, H., Adatte, H., Bolle, M.–.P., 2003b. Late Palaeocene–early Eocene Dinoflagellate Cyst Records from the Tethys; Further Observations on the Global Distribution of *Apectodinium*. In: Wing, S., Gingerich, P.D., Schmitz, B., Thomas, E. (Eds.), Causes and Consequences of Globally Warm Climates in the Early Paleogene: Geol. Soc. Am. Spec. Pap., vol. 369. Geological Society of America Inc., Boulder, Colorado, pp. 113–131.

Cui, Y., 2010. Carbon addition during the Paleocene–Eocene thermal maximum: model inversion of a new, high-resolution carbon isotope record from Svalbard. Masters Thesis (unpublished), Pennsylvania State University, Pennsylvania.

Dallmann, W.K., Midbø, P.S., Nøttvedt, A., Steel, R.J., 1999. Tertiary Lithostratigraphy. In: Dallmann, W.K. (Ed.), Lithostratigraphic Lexicon of Svalbard. Norsk Polarinstitutt, Tromsø, pp. 215–263.

DeConto, R.M., Pollard, D., 2003. Rapid Cenozoic glaciation of Antarctica induced by declining atmospheric CO_2. Nature 421, 245–249.

Dickens, G.R., O'Neil, J.R., Rea, D.K., Owen, R.M., 1995. Dissociation of oceanic methane hydrate as a cause of the carbon isotope excursion at the end of the Paleocene. Paleoceanography 10, 965–971.

Dypvik, H., Riber, L., Burca, F., Rüther, D., Jargvoll, D., Nagy, J., Jochmann, M., in press. The Paleocene-Eocene thermal maximum (PETM) in Svalbard – clay mineral and geochemical signals. Palaeogeog. Palaeoclimat. Palaecol.

Fensome, R.A., Williams, G.L., 2004. *The Lentin and Williams Index of Fossil Dinoflagellates, 2004 Edition.* Am. Assoc. Stratigr. Palynol., Contribution Series 42, Austin, Texas.

Gavrilov, Y.O., Shcherbinina, E.A., Oberhänsli, H., 2003. Paleocene–Eocene Boundary Events in the Northeastern Peri-Tethys. In: Wing, S., Gingerich, P.D., Schmitz, B., Thomas, E. (Eds.), Causes and Consequences of Globally Warm Climates in the Early Paleogene: Geol. Soc. Am. Spec. Paper, vol. 369. Geological Society of America Inc., Boulder, Colorado, pp. 147–168.

Gibbs, R.J., 1977. Clay mineral aggregation in the marine environment. J. Sediment. Petrol. 47, 237–243.

Gibson, T.G., Bybell, L.M., Owens, J.P., 1993. Latest Paleocene lithologic and biotic events in neritic deposits of southwestern New Jersey. Paleoceanography 8, 495–514.

Gibson, T.G., Bybell, L.M., Mason, D.B., 2000. Stratigraphic and climatic implications of clay mineral changes around the Palaeocene/Eocene boundary of the northeastern US margin. Sediment. Geol. 134, 65–92.

Greenwood, D.R., Wing, S.L., 1995. Eocene continental climates and latitudinal temperature gradients. Geology 23, 1044–1048.

Handley, L., Pearson, P.N., McMillan, I.K., Pancost, R.D., 2008. Large terrestrial and marine carbon and hydrogen isotope excursions in a new Paleocene/Eocene boundary section from Tanzania. Earth Planet. Sci. Lett. 275, 17–25.

Hardenbol, J., 1994. Sequence stratigraphic calibration of Paleocene and lower Eocene continental margin deposits in NW Europe and the US Gulf Coast with the oceanic chronostratiraphic record. Geol. Fören. Stockh. Förh. 116, 49–51.

Harland, W., 1997. Palaeogene History of Svalbard. In: Harland, B. (Ed.), The Geology of Svalbard: Mem. Geol. Soc. London, vol. 17, pp. 388–417.

Iakovleva, A.I., Brinkhuis, H., Cavagnetto, C., 2001. Late Palaeocene-Early Eocene dinoflagellate cysts from the Turgay Strait, Kazakhstan; correlations across ancient seaways. Palaeogeogr. Palaeoclimat. Palaeoecol. 172, 243–268.

Jenkins, C.D., 2000. The ecological significance of foraminifera in the Kimmeridgian of Southern England. Grzybowski Found. Spec. Pub. 7, 167–178.

John, C.M., Bohaty, S.M., Zachos, J.C., Sluijs, A., Gibbs, S., Brinkhuis, H., Bralower, T., 2008. North American continental margin records of the Palaeocene–Eocene Thermal Maximum: implications for global carbon and hydrological cycling. Paleoceanography 23. doi:10.1029/2007PA001465.

Please cite this article as: Harding, I.C., et al., Sea-level and salinity fluctuations during the Paleocene–Eocene thermal maximum in Arctic Spitsbergen, Earth Planet. Sci. Lett. (2011), doi:10.1016/j.epsl.2010.12.043

Kelly, D.C., Bralower, T.J., Zachos, J.C., Premoli-Silva, I., Thomas, E., 1996. Rapid diversification of planktonic foraminifera in the tropical Pacific (ODP Site 865) during the late Paleocene Thermal Maximum. Geology 24, 423–426.
Kennett, J.P., Stott, L., 1991. Abrupt deep-sea warming, palaeoceanographic changes and benthic extinctions at the end of the Palaeocene. Nature 353, 225–229.
Kirschvink, J.L., 1980. The least squares line and plane and the analysis of palaeomagnetic data. Geophys. J. Roy. Astron. Soc. 62, 699–718.
Knies, J., Mann, U., Popp, B.N., Stein, R., Brumsack, H.–J., 2008. Surface water productivity and paleoceanographic implications in the Cenozoic Arctic Ocean. Paleoceanography 23. doi:10.1029/2007PA001455.
Koch, P.L., Zachos, J.C., Gingerich, P.D., 1992. Correlation between isotope records in marine and continental carbon reservoirs near the Palaeocene/Eocene boundary. Nature 358, 319–322.
Koch, P.L., Zachos, J.C., Dettman, D.L., 1995. Stable isotope stratigraphy and paleoclimatology of the Paleogene Bighorn Basin (Wyoming, USA). Palaeogeogr. Palaeoclimatol. Palaeoecol. 115, 61–89.
Magioncalda, R., Dupuis, C., Smith, T., Steurbaut, E., Gingerich, P.D., 2004. Paleocene–Eocene carbon isotope excursion in organic carbon and pedogenic carbonate: direct comparison in a continental stratigraphic section. Geology 32, 553–556.
Manum, S.B., Throndsen, T., 1986. Age of Tertiary formations on Spitsbergen. Polar Res. 4, 103–131.
Markwick, P.J., 1998. Fossil crocodilians as indicators of Late Cretaceous and Cenozoic climates: implications for using palaeontological data in reconstructing palaeoclimate. Paleogeog. Paleoclim. Paleoecol. 137, 205–271.
Miller, K.G., Mountain, G.S., Browning, J.V., Kominz, M., Sugarman, P.J., Christie-Blick, N., Katz, M.E., Wright, J.D., 1998. Cenozoic global sea level, sequences, and the New Jersey transect: results from coastal plain and continental slope drilling. Rev. Geophys. 36, 569–601. doi:10.1029/98RG01624.
Miller, K.G., Kominz, M.A., Browning, J.V., Wright, J.D., Mountain, G.S., Katz, M.E., Sugarman, P.J., Cramer, B.S., Christie-Blick, N., Pekar, S.F., 2005. The Phanerozoic record of sea-level change. Science 310, 1293–1298.
Moran, K., Backman, J., Brinkhuis, H., Clemens, S., Cronin, T., Dickens, G., Eynaud, F., Gattacceca, J., Jakobsson, M., Jordan, R., Kaminski, R., King, J., Koc, N., Krylov, A., Martinez, N., Matthiessen, J., McInroy, D., Moore, T., Onodera, J., O'Regan, M., Pälike, H., Rea, B., Rio, D., Sakamoto, T., Smith, D., Stein, R., St John, C., Suto, I., Suzuki, N., Takahashi, K., Watanabe, M., Yamamoto, M., Farrell, J., Frank, M., Kubik, P., Jokat, W., Kristoffersen, Y., 2006. The Cenozoic palaeoenvironment of the Arctic Ocean. Nature 441, 601–605.
Mosar, J., Torsvik, T.H., BAT team, 2002. Opening of the Norwegian and Greenland Seas: Plate Tectonics in Mid Norway since the Late Permian. In: Eide, E.A. (Ed.), BATLAS — Mid Norway plate reconstructions atlas with global and Atlantic perspectives: Geol. Surv. Norway, pp. 48–59.
Pagani, M., Pedentchouk, N., Huber, M., Sluijs, A., Schouten, S., Brinkhuis, H., Sinninghe Damsté, J.S., Dickens, G.R., Expedition 302 Scientists, 2006. Arctic hydrology during global warming at the Palaeocene/Eocene Thermal Maximum. Nature 442, 671–675.
Pälike, H., Spofforth, D.J.A., O'Regan, M., Gattacceca, J., 2008. Orbital scale variations and timescales from the Arctic Ocean. Paleoceanography 23. doi:10.1029/2007PA001490.
Powell, A.J., Brinkhuis, H., Bujak, J.P., 1996. Upper Paleocene–lower Eocene Dinoflagellate Cyst Sequence Biostratigraphy of South-east England. In: Knox, R.W., Dunay, R. E., Corfield, R.M. (Eds.), Correlation of the Early Paleogene in Northwest Europe: Geol. Soc. London Spec. Publ., vol. 101, pp. 145–183.
Raffi, I., Backman, J., Pälike, H., 2005. Changes in calcareous nannofossil assemblages across the Palaeocene/Eocene transition from the paleo-equatorial Pacific Ocean. Paleogeogr. Paleoclimatol. Paleoecol. 226, 93–126.
Robert, C., Chamley, H., 1991. Development of early Eocene warm climates, as inferred from clay mineral variation in oceanic sediments. Glob. Planet. Change 3, 315–332.
Robert, C., Kennett, J.P., 1992. Paleocene/Eocene kaolinite distribution in the South Atlantic and Southern Ocean: Antarctic climatic and paleoceanographic implications. Mar. Geol. 103, 99–110.
Robert, C., Kennett, J.P., 1994. Antarctic subtropical humid episode at the Paleocene–Eocene boundary: clay-mineral evidence. Geology 22, 211–214.
Röhl, U., Westerhold, T., Bralower, T.J., Zachos, J.C., 2007. On the duration of the Paleocene–Eocene Thermal Maximum (PETM). Geochem. Geophys. Geosyst. 8. doi:10.1029/2007/GC001784.
Schouten, S., Woltering, M., Rijpstra, I.C., Sluijs, A., Brikhuis, H., Sinninghe Damsté, J.S., 2007. The Paleocene–Eocene carbon isotope excursion in higher plant organic matter: differential fractionation of angiosperms and conifers in the Arctic. Earth Planet. Sci. Lett. 258, 581–592.
Schultz, L.G., 1964. Quantitative interpretation of mineralogical composition from X-ray and chemical data for the PierreShale. U.S. Geol. Surv. Prof. Pap. 391 C, 1–31.
Sluijs, A., Brinkhuis, H., 2009. A dynamic climate and ecosystem state during the Paleocene–Eocene Thermal Maximum: inferences from dinoflagellate cyst assemblages on the New Jersey Shelf. Biogeosciences 6, 1755–1781.
Sluijs, A., Schouten, S., Pagani, M., Woltering, M., Brinkhuis, H., Sinninghe Damsté, J.S., Dickens, G.R., Huber, M., Reichart, G.J., Stein, R., Matthiessen, J., Lourens, L.J., Pedentchouk, N., Backman, J., Moran, K., Expedition 302 Scientists, 2006. Subtropical Arctic Ocean temperatures during the Palaeocene–Eocene Thermal Maximum. Nature 441, 610–613.
Sluijs, A., Bowen, G.J., Brinkhuis, H., Lourens, L.J., Thomas, E., 2007b. The Palaeocene–Eocene Thermal Maximum Super Greenhouse: Biotic and Geochemical Signatures, Age Models and Mechanisms of Global Change. In: Williams, M., Hayward, A.M., Gregory, F. J., Schmidt, D.N. (Eds.), Deep Time Perspectives on Climate Change: Marrying the Signal from Computer Models and Biological Proxies. The Micropalaeontological Society, Special Publications. Geol. Soc. London, London, pp. 323–349.
Sluijs, A., Brinkhuis, H., Schouten, S., Bohaty, S.M., John, C.M., Zachos, J.C., Reichart, G., Sinninghe Damste, J.S., Crouch, E.M., Dickens, G.R., 2007a. Environmental precursors to rapid light carbon injection at the Palaeocene/Eocene boundary. Nature 450, 1218–1221.
Sluijs, A., Röhl, U., Schouten, S., Brumsack, H., Sangiorgi, F., Sinninghe Damsté, J.S., Brinkhuis, H., 2008a. Arctic late Paleocene–early Eocene paleoenvironments with special emphasis on the Paleocene–Eocene Thermal Maximum (Lomonosov Ridge, Integrated Ocean Drilling Program Expedition 302). Paleoceanography 23. doi:10.1029/2007PA001495.
Sluijs, A., Brinkhuis, H., Crouch, E.M., John, C.M., Handley, L., Munsterman, D., Bohaty, S.M., Zachos, J.C., Reichart, G., Schouten, S., Pancost, R.D., Sinninghe Damsté, J., Welters, N.L.D., Lotter, A.F., Dickens, G.R., 2008b. Eustatic variations during the Palaeocene–Eocene greenhouse world. Paleoceanography 23. doi:10.1029/2008PA001615.
Smith, T., Rose, K.D., Gingerich, P.D., 2006. Rapid Asia-Europe-North America geographic dispersal of earliest Eocene primate *Teilhardina* during the Paleocene-Eocene thermal maximum. Proc. Natl Acad. Sci. 103, 11223–11227.
Smith, F.A., Wing, S.L., Freeman, K.H., 2007. Magnitude of the carbon isotope excursion at the Paleocene–Eocene thermal maximum: the role of plant community change. Earth Planet. Sci. Lett. 262, 50–65.
Speijer, R.P., Morsi, A.M., 2002. Ostracod turnover and sea-level changes associated with the Paleocene–Eocene thermal maximum. Geology 30, 23–26.
Speijer, R.J., Wagner, T., 2002. Sea-level Changes and Black Shales Associated with the Late Paleocene Thermal Maximum: Organic-geochemical and Micropaleontologic Evidence from the Southern Tethyan Margin (Egypt–Israel). In: Koeberl, C., MacLeod, K.G. (Eds.), Catastrophic Events and Mass Extinctions: Impacts and Beyond: Geol. Soc. Am. Spec. Pap., vol. 356. Geological Society of America Inc., Boulder, Colorado, pp. 533–549.
Stein, R., Boucsein, B., Meyer, H., 2006. Anoxia and high primary productivity in the Palaeogene central Arctic Ocean: first detailed records from Lomonosov Ridge. Geophys. Res. Lett. 33. doi:10.1029/2006GL026776.
Steurbaut, E., Magioncalda, R., Dupuis, C., Van Simaeys, S., Roche, E., Roche, M., 2003. Palynology, Paleoenvironments, and Organic Carbon Isotope Evolution in Lagoonal Paleocene-Eocene Boundary Settings in North Belgium. In: Wing, S., Gingerich, P.D., Schmitz, B., Thomas, E. (Eds.), Causes and Consequences of Globally Warm Climates in the Early Paleogene: Geol. Soc. Am. Spec. Pap., vol. 369. Geological Society of America Inc., Boulder, Colorado, pp. 291–317.
Stockmarr, J., 1972. Tablets with spores used in absolute pollen analysis. Pollen Spores 13, 615–621.
Thomas, E., 1998. Biogeography of the late Paleocene benthic foram extinction. In: Aubry, M.-P., Lucas, S.G., Berggren, W.A. (Eds.), Late Palaeocene–Early Eocene Biotic and Climatic Events in Marine and Terrestrial Records. Columbia University Press, New York, pp. 214–243.
Thomas, E., Shackleton, N.J., 1996. The Paleocene–Eocene Benthic Foraminiferal Extinction and Stable Isotope Anomalies. In: Knox, R.W., Dunay, R.E., Corfield, R.M. (Eds.), Correlation of the Early Paleogene in Northwest Europe: Geol. Soc. London Spec. Publ., vol. 101, pp. 401–441.
Thomas, D.J., Zachos, J.C., Bralower, T.J., Thomas, E., Bohaty, S., 2002. Warming the fuel for the fire: evidence for the thermal dissociation of methane hydrate during the Paleocene–Eocene thermal maximum. Geology 30, 1067–1070.
Tripati, A., Elderfield, H., 2005. Deep-sea temperature and circulation changes at the Paleocene–Eocene thermal maximum. Science 308, 1894–1898.
Tripati, A., Zachos, J.C., Marincovich Jr., L., Bice, K., 2001. Late Palaeocene Arctic coastal climate inferred from molluscan stable and radiogenic isotope ratios. Paleogeogr. Paleoclimatol. Paleoecol. 170, 101–113.
Tyson, R.V., 1995. Sedimentary organic matter: organic facies and palynofacies. Chapman and Hall, London. 615 pp.
Waddell, L.M., Moore, T.C., 2008. Salinity of the Eocene Arctic Ocean from oxygen isotope analysis of fish bone carbonate. Paleoceanography 23. doi:10.1029/2007PA001451.
Weijers, J.W.H., Schouten, S., Sluijs, A., Brinkhuis, H., Sinninghe Damsté, J.S., 2007. Warm Arctic continents during the Palaeocene–Eocene thermal maximum. Earth Planet. Sci. Lett. 261, 230–238.
Weller, P., Stein, R., 2008. Palaeogene biomarker records from the central Arctic Ocean (Integrated Ocean Drilling Program Expedition 302): organic carbon sources, anoxia, and sea surface temperature. Paleoceanography 23. doi:10.1029/2007PA001472.
Westerhold, T., Röhl, U., Laskar, J., Raffi, I., Bowles, J., Lourens, L.J., Zachos, J.C., 2007. On the duration of magnetochrons C24r and C25n and the timing of early Eocene global warming events: implications from the Ocean Drilling Program Leg 208 Walvis Ridge depth transect. Paleoceanography 22, PA2201. doi:10.1029/2006PA001322.
Westerhold, T., Röhl, U., McCarren, H.K., Zachos, J.C., 2009. Latest on the absolute age of the Paleocene–Eocene thermal maximum (PETM): new insights from exact stratigraphic position of key ash layers +19 and −17. Earth Planet. Sci. Lett. 287, 412–419.
Wing, S.L., Harrington, G.J., Smith, F.A., Bloch, J.I., Boyer, D.M., Freeman, K.H., 2005. Transient floral change and rapid global warming at the Paleocene–Eocene boundary. Science 310, 993–996.
Zachos, J.C., Pagani, M., Sloan, L., Thomas, E., Billups, K., 2001. Trends, rhythms, and aberrations in global climate 65 Ma to present. Science 292, 686–693.
Zachos, J.C., Wara, M.W., Bohaty, S., 2003. A transient rise in tropical sea surface temperature during the Palaeocene–Eocene Thermal Maximum. Science 302, 1551–1554.
Zachos, J.C., Röhl, U., Schellenberg, S.A., Sluijs, A., Hodell, D.A., Kelly, D.C., Thomas, E., Nicolo, M., Raffi, I., Lourens, L.J., McCarren, H., Kroon, D., 2005. Rapid acidification of the ocean during the Palaeocene–Eocene thermal maximum. Science 308, 1611–1615.
Zachos, J.C., Schouten, S., Bohaty, S., Quattlebaum, T., Sluijs, A., Brinkhuis, H., Gibbs, S., Bralower, T., 2006. Extreme warming of the mid-latitude coastal ocean during the Paleocene–Eocene Thermal Maximum: inferences from TEX_{86} and isotope data. Geology 34, 737–740.

Please cite this article as: Harding, I.C., et al., Sea-level and salinity fluctuations during the Paleocene–Eocene thermal maximum in Arctic Spitsbergen, Earth Planet. Sci. Lett. (2011), doi:10.1016/j.epsl.2010.12.043